Journal of Photochemistry and Photobiology 8 (2021) 100078

Contents lists available at ScienceDirect

Journal of Photochemistry and Photobiology

journal homepage: www.sciencedirect.com/journal/journal-of-photochemistry-and-photobiology

Photophysical properties of a β-Carboline Rhenium (I) complex. Solvent effects on excited states and their redox reactivity

Iván Maisuls [a,b], Ezequiel Wolcan [a], Pedro M. David-Gara [c], Franco M. Cabrerizo [b], Guillermo J. Ferraudi [d], Gustavo T. Ruiz [a,*]

[a] Instituto de Investigaciones Fisicoquímicas Teóricas y Aplicadas (INIFTA, UNLP, CCT La Plata-CONICET), Diag. 113 y 64, Sucursal 4, C.C. 16, (B1906ZAA) La Plata, Argentina
[b] Instituto Tecnológico de Chascomús (INTECH, UNSAM, CONICET), Intendente Marino Km 8.2, CC 164 (B7130IWA), Chascomús, Argentina
[c] Centro de Investigaciones Ópticas (CIOP, CONICET, CIC), Universidad Nacional de La Plata, CC.3, (1897), La Plata, Argentina
[d] Radiation Research Building, University of Notre Dame, Notre Dame, IN 46556, United States

ARTICLE INFO

Keywords:
Rhenium tricarbonyl complexes
Singlet oxygen generation
Photophysics
Photochemistry
Norharmane – TD-DFT
Pulse radiolysis

ABSTRACT

The photochemical and photophysical properties of a *Re*(I) tricarbonyl complex, $ClRe(CO)_3(nHo)_2$, where nHo = 9H-pyrido[3,4-b] indole (norharmane), were investigated in solution phase by a combination of steady state emission spectroscopy, laser flash photolysis (LFP) and pulse radiolysis (PR) techniques. These results allowed us to identify and study the reactivity of the β-carboline (nHo) Rhenium(I) complex main excited states. The absorption spectrum as well as the steady-state and time-resolved luminescence of the complex exhibits a marked dependence with the solvent properties. These experimentally observed results were corroborated by quantum chemical calculations, TD-DFT. The most important electronic transitions present in the spectrum in all solvents are $MLLCT_{Re(CO)3\rightarrow nHo1,\ nHo2}$ along with a mixture of IL_{nHo} and $LLCT_{Cl\rightarrow nHo}$ transitions. The relationship between the dipole moment and the polarity of the solvent was rationalized in terms of the electron density inside and outside the complex. While the luminescence of the complex is mainly attributed to the emitting $^1IL_{nHo}$ state, in LFP experiments a MLCT excited state was also detected. The species generated in either reductive or oxidative conditions in LFP experiments were compared with those obtained in PR. Also, the quenching rate constant (k_q) of the excited state with MV^{+2} was calculated. The excited state of the complex can efficiently generate singlet oxygen in acetonitrile yielding a $\Phi_\Delta = 0.25 \pm 0.02$. Optoacoustic measurements showed that, after photonic excitation, almost all the absorbed energy by the complex is released to the medium as prompt heat. The investigated photophysical and photochemical properties of $ClRe(CO)_3(nHo)_2$ are of significant importance in relation to the use of this β-carboline Rhenium(I) complex in several biomedical fields, such as photodynamic therapy and photoactivated chemotherapy as well as new alternative therapies such as regional hyperthermia.

1. Introduction

β-Carbolines (βCs) are a group of alkaloids widely spread in nature. Their presence has been suggested in several plant and animal species, displaying a pharmacological functions including antioxidants, antitumor, antiviral and antimicrobial activities, among many others [1–10]. In addition, these biological activities can be enhanced or triggered by light [11–17].

As it is widely known, the combination of light-sensitive bioactive ligands such as βCs with transition metals permits the design of innovative compounds that can optimize or enhance the intrinsic photochemical, photophysical, or photobiological properties of the non-coordinated βC molecules [18–22]. Recent work from a few research groups has shown the potential anticancer properties of different β-carboline metal complexes [23]. The nature of metal core strongly modulates the multi-mechanistic anticancer activities as well as the selective toxicity against different cancer cell lines. In addition, the type of transition metal bound to the βC derivative induce distinctive photophysical properties [24–28]. In particular, Rhenium (I) tricarbonyl complexes with different polypyridines as bidentate ligands, in addition to on βC moiety placed as an ancillary ligand, represent a set of metal complexes with quite promising photophysical and photobiological

* Corresponding author.
E-mail address: gruiz@inifta.unlp.edu.ar (G.T. Ruiz).

https://doi.org/10.1016/j.jpap.2021.100078
Received 27 June 2021; Received in revised form 29 September 2021; Accepted 21 October 2021
Available online 28 October 2021
2666-4690/© 2021 The Authors. Published by Elsevier B.V. This is an open access article under the CC BY-NC-ND license (http://creativecommons.org/licenses/by-nc-nd/4.0/).

properties. We have shown, for example, the differential capabilities of this kind of complexes to induce (or photoinduce) DNA damage [29,30]. In general, *Re*(I) complexes offer numerous advantages over other metal coordination compounds such as thermal and photochemical stability and an exceptionally rich excited-state and thermal redox chemistry behavior, among others [29,31–35]. In addition, the accessible excited states of *Re*(I) tricarbonyl complexes, such as metal to ligand charge transfer ($MLCT_{Re\rightarrow L}$) and/or intraligand (IL) excited states, are generally long-lived and luminescent at room temperature [36–39]. These conditions allow us to investigate the photophysical processes in which these excited states are involved as well as their redox reactivity [29, 40–43]. Besides, *Re*(I) complexes has been proposed, also, as promising candidates in anticancer treatments and as biological probes [44–50].

While there are scarcely reported *Re*(I) complexes with βCs as ligands present in the bibliography, in all the recorded complexes the photophysical properties of the compounds were commanded by the bidentate accompanying luminophore [25,26,51]. In those complexes, the βC derivative was acting only as a spectator ligand, with a minor photophysical role when compared with the other moieties.

Therefore, in this work, we undertook a deep photophysical and photochemical study of a *Re*(I) complex with βCs as the only type of constitutive ligand, $ClRe(CO)_3(nHo)_2$ where nHo = norharmane, to avoid the influence of any additional ligands, (Scheme 1) [25].

Although we have recently shown that the most important electronic transitions present in the absorption spectrum of this complex are metal to ligand charge transfer ($MLCT_{Re->nHo}$) along with a mixture of intraligand (IL_{nHo}) and ligand to ligand charge transfer ($LLCT_{Cl->nHo}$) transitions by TDDFT calculations [25], in this work we extend the studies on the experimental photophysical behavior of solutions of $ClRe(CO)_3(nHo)_2$ complex in solvents of different polarity. We also present their photoluminescence properties (such as excited state photoluminescence lifetimes, emission spectra, and quantum yields) in different solvents, and these experimental results were complemented through theoretical calculations. With the assistance of laser flash photolysis (LFP) and pulse radiolysis (PR) techniques, we performed a full analysis of the possible excited state species and/or radicals derived from the complex after a pulse of light or electrons. Furthermore, the excited state's redox properties of the complex were examined by both reductive and oxidative quenching. Finally, the ability of the complex to generate singlet oxygen was evaluated as well as their skill to release heat through laser-induced optoacoustic spectroscopy (LIOAS) measurements.

2. Methods and materials

2.1. General

$ClRe(CO)_3(nHo)_2$ (***Re*(nHo)$_2$**) and Methyl-Viologen (MV^{+2}) were available from previous works [25,52]. Norharmane, 2-hydroxybenzophenone and phenalenone were purchased from Sigma Aldrich at the highest purity available and were used as received. Spectrograde and HPLC grade acetonitrile (ACN), dichloromethane (DCM), ethanol (EtOH), dimethylsulfoxide (DMSO), tetrahydrofuran (THF), toluene (Tol), acetone (Ace) and triethylamine (TEA) were purchased to Sigma-Aldrich and used without further purification. Methanol (MeOH), benzene (BzH) and carbon tetrachloride (CCl_4) were purchased to Merck and K_2HPO_4 to J.T. Baker.

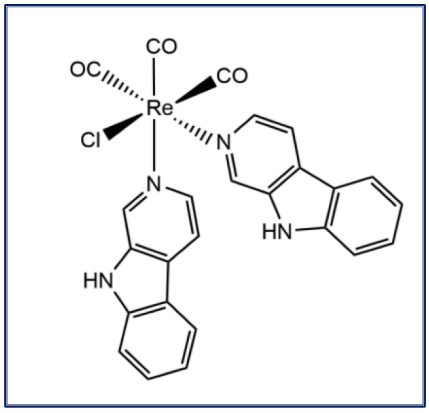

Scheme 1. Structure of $ClRe(CO)_3(nHo)_2$ (***Re*(nHo)$_2$**).

2.2. Solutions with methyl-viologen

Methanolic solutions of ***Re*(nHo)$_2$** with different concentrations of MV^{+2} were prepared by adding different volumes of MV^{+2} (10^{-4} M) to the complex solution, reaching a final volume of 10 ml. The concentration of the complex (10^{-5} M) was kept constant in all experiments.

2.3. Photochemical and photophysical measurements

UV−vis spectra were recorded on a Shimadzu UV-1800 spectrophotometer. Emission spectra were obtained with a computer-interfaced Near-IR Fluorolog-3 Research Spectrofluorometer and were corrected for differences in spectral response and light scattering. Solutions were deaerated with O_2-free N_2 in a gas-tight cell before recording the spectra. Luminescence lifetime measurements were carry out using a nanoLED, λ_{ex} = 341 nm, as excitation source. Photoluminescence quantum yields, Φ_F, were calculated using eq. (1).

$$\varnothing_F = \frac{A_{ref} I_F n_F^2}{A_F I_{ref} n_{ref}^2} \varnothing_{ref} \quad (1)$$

where A is the absorbance of the sample, I is the intensity of the luminescence calculated as the integral under the entire emission spectra, Φ_{ref} is the quantum yield of the reference and n is the refractive index of the solvent. For the experiments, nHo (Φ_{ref} = 0.30 in MeOH) was used as reference [53–55].

2.4. Flash photolysis and pulse radiolysis

Absorbance changes, ΔA, occurring in a time scale longer than 10 ns were investigated with a flash photolysis apparatus described elsewhere [56,57]. In these experiments, 10 ns flashes of 351 nm light were generated with a Lambda Physik SLL −200 excimer laser. The energy of the laser flash was attenuated to values equal to or less than 20 mJ/pulse by absorbing some of the laser light in a filter solution of $Ni(ClO_4)_2$ having the desired optical transmittance, $T = I_t / I_0$ where I_0 and I_t are respectively the intensities of the light arriving to and transmitted from the filter solution. The transmittance, $T = 10^{-A}$, was routinely calculated by using the spectrophotometrically measured absorbance, A, of the filter solution. A right-angle configuration was used for the pump and the probe beams. Concentrations of the photolytes were adjusted to provide homogeneous concentrations of photogenerated intermediates over the optical path, l = 1 cm, of the probe beam. To satisfy this optical condition, solutions were made with an absorbance equal to or less than 0.8 over the 0.2 cm optical path of the pump.

Pulse radiolysis experiments were carried out with a model TB-8/16–1S electron linear accelerator, LINAC. The instrument and computerized data collection for time-resolved UV–Vis spectroscopy and reaction kinetics have been described elsewhere in the literature [58,59]. Thiocyanate dosimetry was carried out at the beginning of each experimental session. The details of the dosimetry have been reported elsewhere [60]. The procedure is based on the concentration of $(SCN)_2^{\bullet}$ radicals generated by the electron pulse in a N_2O saturated 10^{-2} M SCN^- solution. In the procedure, the calculations were made with G = 6.13 and an extinction coefficient, $\varepsilon = 7.58 \times 10^3\ M^{-1}\ cm^{-1}$ at 472 nm, for the $(SCN)_2^{\bullet}$ radicals [58,60]. In general, the experiments were carried

out with doses that in N_2 saturated aqueous solutions resulted in $(2.0 \pm 0.1) \times 10^{-6}$ M to $(6.0 \pm 0.3) \times 10^{-6}$ M concentrations of e^-_{solv}. In all the experiments, solutions in methanol were deaerated under vacuum in a gas-tight cell. In methanolic solutions, the radiolytic pulse yield e^-_{solv} and $C^{\bullet}H_2OH$ radicals according to the following reactions scheme 2:

Thereby, in pulse radiolysis of methanolic solutions under an N_2 atmosphere, the main reducing species formed are e^-_{solv} and $C^{\bullet}H_2OH$ [60]. As these species have large reduction potentials (−0.92 V for $C^{\bullet}H_2OH$ and −2.8 V for e^-_{solv}, both against NHE [61]) they have been used for the study of both electron transfer and reduction reactions of different species like coordination complexes of different transition metals. The G-value of e^-_{solv} in MeOH ($G \approx 1.2$) is approximately one-third part of the yield in the radiolysis of H_2O ($G \approx 2.8$). When the e^-_{solv} is scavenged with N_2O, the $C^{\bullet}H_2OH$ radical is the predominant product (yield >90%) of the reaction between $O^{\bullet-}$ and CH_3OH. The reaction kinetics were investigated by following the absorbance change at given wavelengths of the spectrum and incorporating those changes in the dimensionless parameter ξ, according to eq. (2).

$$\xi = \frac{\Delta A_{inf} - \Delta A_t}{\Delta A_{inf} - \Delta A_0} \quad (2)$$

where ΔA_0, ΔA_t *and* ΔA_{inf} are the absorbance changes at the beginning of the reaction, at a given time t, and at the end of the reaction, respectively.

2.5. Singlet oxygen production and optoacoustic measurements

The experimental details of this technique have been published previously [62]. Briefly, quantum yields of photosensitized singlet oxygen production, Φ_Δ, were obtained using the third harmonic of a Q-switched Nd-YAG laser as the excitation source (λ_{ex} = 355 nm, Surelite II- Continuum), looking at the 1270 nm $^1O_2$ phosphorescence with a Ge-photodiode (Applied Detector Corporation, resolution time of 1 μs). Measurements were performed in air-equilibrated solutions. The averages of signals generated by 64 laser shots were recorded to improve the signal-to-noise ratio. Single exponential analysis of emission decays was performed with the exclusion of the initial part of the signal. Φ_Δ was determined by measuring its phosphorescence intensity using an optically matched solution of a reference sensitizer. In acetonitrile, the reference used was phenalenone (Φ_Δ =0.975) [63].

Photoacoustic measurements were performed by using a set-up already described [62]. The resolution time in our experimental set-up, t_R, was ca. 800 ns [62]. 2-hydroxybenzo-phenone was used as calorimetric reference (CR) compounds in ACN solutions [64,65]. Experiments were performed under a controlled atmosphere, bubbling N_2 or O_2 in the solution, for 15 min. In principle, all the excited species with lifetimes $t \leq$ ⅕ t_R release their heat content as prompt heat, whereas excited species with a lifetime of $\tau \geq 5\ t_R$ function as heat storage within the time resolution of the LIOAS experiment. For the handling of the LIOAS signals, eq. (3) was used, which relates the peak to peak amplitude of the first optoacoustic signal (H) with the fraction of the excitation laser fluence (*F*) absorbed by the sample [66].

$$H = K\alpha F\left(1 - 10^{-A}\right) \quad (3)$$

where *K* is the experimental constant that contains the thermo-elastic parameters of the solution as well as instrumental factors, *A* is the absorbance of the sample at λ_{ex} and *a* is the fraction of the energy released to the medium as prompt heat within the time resolution of the experiment.

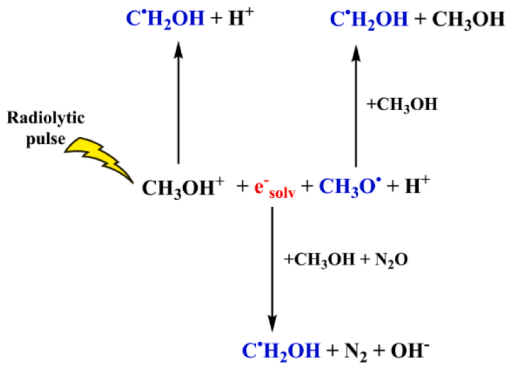

Scheme 2. Generated MeOH-derived species after the radiolytic pulse.

3. Results and discussion

3.1. UV–Vis spectroscopy

Fig. 1 shows the solvent dependence of the spectral features of ***Re*(nHo)$_2$** in solvents of different polarities. As observed, the intense band centered at $\lambda_{max} \sim 240$ nm is practically not affected by the solvent, as depicted also in Table 1. In contrast, the lower energy absorption band experiences a bathochromic shift and an intensity decrease as the dielectric constant (ε) drops. The latter fact was further explored with an additional group of solvents, showing a clear correlation between the wavelength of the lower energy band with the solvent dielectric constant (Figure S1a). Similar spectroscopic behavior observed previously in the non-coordinated nHo indicates a strong interaction of the solvent with the ligand [53,67] .

A comparative analysis of the absorption spectra of the complex in methanolic solutions with those recorded for non-coordinated neutral (nHo) and protonated ($nHoH^+$) norharmane (Fig. 1), clearly evidenced that, despite other electronic transitions, both nHo-like (probably to a greater extent) and $nHoH^+$-like βC's rings contribute, at least in part, to the overall absorption of ***Re*(nHo)$_2$** [25,53,67,68]. In addition, new charge transfer transitions must be present also at λ > 300 nm due to the coordination of the βC molecule to *Re*(I) metal.

It should be noted that although the recorded spectra show that the highest energy band is rather insensitive to the polarity of the solvent while the band centered at ~310 nm experiences a bathochromic shift when the polarity of the solvent decreases, this effect is not seen with DMSO (Figure S1a). This fact pinpoints to a probable specific interaction between DMSO and the *Re*(I) complex which was not taken account in the theoretical calculations presented below.

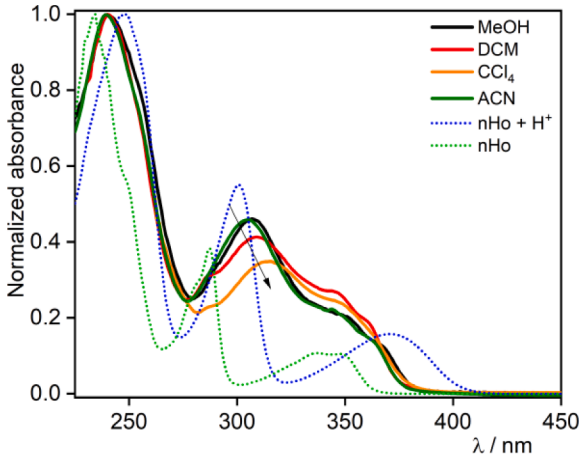

Fig. 1. Normalized UV–Vis spectra of ***Re*(nHo)$_2$** in different solvents (solid lines). For comparison, non-coordinated nHo and $nHoH^+$ in neutral and acidic organic solvent (green and blue dotted lines, respectively) are also shown. Absorption coefficients are displayed in Figure S1b.

Table 1
λ_{max} of ***Re*(nHo)$_2$** in different solvents and dipole moment (μ) and dielectric constant (ε) of the solvents [69].

Solvent	λ_{max}, nm	λ_{max}, nm	μ, D (debye)	ε at 25 °C
CH_3CN	239	305	3.53 (at 25 °C)	35.94
CH_3OH	241	307	2.87 (at 20 °C)	32.66
CH_2Cl_2	241	309	1.14	8.93
CCl_4	—	315	0	2.23

3.2. Quantum chemistry of Re(nHo)$_2$

To get a deeper understanding of the absorption spectrum of *Re*(nHo)$_2$ and its dependence with the solvent described above, a systematic TD-DFT theoretical study is present herein. To this aim, spectra were simulated under 10 different solvents (i.e., PCM = DMSO, ACN, MeOH, EtOH, Ace, DCM, THF, Tol, BzH and CCl4) with different intensive properties. A set of MLCT, LLCT and IL electronic transitions was taken into account in the calculations. The calculations were carried out at the M06/6–311 G/6–311G*/LanL2TZ(f)/PCM level of theory.

Fig. 2 depicts the UV–visible absorption spectra of ***Re*(nHo)$_2$** simulated under both vacuo and the 10 different solvents mentioned above (Figure S1a). The calculated absorption spectra follow the experimental trend showing a clear bathochromic shift of the lowest energy absorption band as the polarity of the solvent decreases while the higher energy band experiences hardly any shift. In addition, the highest energy band in vacuo is only blue-shifted by 7 nm relative to the solvent media while the lowest energy band in vacuo is displaced by 20–40 nm to the red relative to its position under the PCM. Electronic transitions results calculated at the same level of theory in vacuo, BzH, and DMSO are summarized in Tables S1-S3. The most relevant MOs which are responsible for the electronic transitions in the absorption spectroscopy of ***Re*(nHo)$_2$** in the 230–500 nm wavelength range are: HOMO, LUMO, and the groups of MOs H-10 through H-1 and *L* + 1 through *L* + 6. The percentage compositions of those MOs were obtained from Mulliken population analysis with the aid of AOMIX program from contributions of five fragments: (i) *Re* atom, (ii) the three carbonyls, (iii) nHo-1 molecule, (iv) nHo-2 molecule, and (v) Cl atom. Tables S4-S5 show the calculated% compositions of all fragments at each MO for ***Re*(nHo)$_2$** in BzH and DMSO.

In the 330–500 nm region, the most relevant electronic transitions are H→L, H→*L* + 1, H-1→L, H-2→L, and H-2→*L* + 1. Fig. 3 shows the spatial plots of a selection of those MOs of ***Re*(nHo)$_2$** in vacuo, BzH, THF, and DMSO, which give insight into the electronic transitions. Fig. 3 shows that in vacuo, H and H-1 are MOs mostly centered on the *Re* atom with contributions from the three CO while L and *L* + 1 are MOs centered on nHo2 and nHo1, respectively. H-2 is very similar in shape to H-1. Therefore, all the electronic transitions in vacuo in this region of wavelengths are $MLLCT_{(Re(CO)3\rightarrow nHo1,\ nHo2)}$. MO shapes in BzH are very similar to MO shapes in vacuo. In THF, however, H and H-1 have in addition significant contributions from nHo1 and nHo2, respectively. On the other hand, L and *L* + 1 have in THF even contributions from nHo1 and nHo2 and those MOs are widespread between both ligands. In DMSO, the charge density is widespread between *Re*, COs, nHo1, and nHo2 in H and H-1. The solvent effect on MOs charge density is responsible for a decrease of the percentage of charge-transfer transition, CT%, as polarity increases, from 48% in vacuo to nearly 32% in DMSO (see definition of CT% in Supporting Material and Table S6).

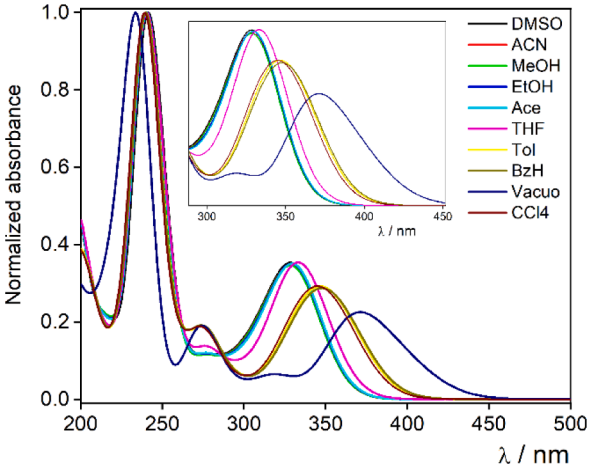

Fig. 2. Simulation of the UV/Vis spectra of ***Re*(nHo)$_2$** in 10 different solvents and *vacuo*. *Inset*: Amplification of the band centered in λ~350 nm.

The decrease in CT% as polarity increases also explains the bathochromic shift of the calculated $MLLCT_{Re(CO)3\rightarrow nHo1,\ nHo2}$ wavelength (λ_{calc}) as solvent polarity decreases. As the charge density over *Re* is lower in DMSO than in BzH, the energy of the $MLLCT_{Re(CO)3\rightarrow nHo1,\ nHo2}$ is higher in DMSO than in BzH and the charge transfer process becomes energetically less feasible. As observed in the previous figures, our calculations are in agreement with the negative solvatochromism observed in less polar solvents. The direction of the solvent dependence is associated with a reduced (and reversed) molecular dipole in their MLCT excited states, as stated in the bibliography [70]. As depicted in the Fig. 4, the molecular dipole moment, μ, increases with the increase on the dielectric constant, ε_r. Moreover, the vector of the dipole moment is directed between the two nHo ligands.

The solvent effect on the dipole moment can be interpreted in terms of electron density plots (Figure S2). In vacuo, the electron density is more concentrated inside the "shape" of the molecule. However, when the polarity of the solvent increases, the electron density becomes more diffuse and it is enhanced outside the molecular limits. Therefore, μ increases.

3.3. Photophysical and photochemical measurements of Re(nHo)$_2$

3.3.1. Luminescence measurements

The emission spectra of ***Re*(nHo)$_2$** were recorded in MeOH, ACN, and DCM (Fig. 5). For comparative purposes, spectra of non-coordinated nHo recorded under different solvent or pH conditions are also shown.

Luminescence spectra of both ***Re*(nHo)$_2$** and non-coordinated nHo, showed a strong solvent dependence. Briefly, a set of three emission bands centered 370–400 nm, 400–480 nm, and 480–550 nm. While the lowest energy transition could be associated to MLCT transitions, the spectrum of non-coordinated nHo suggests a dominant contribution of IL_{nHo} transition [25,67,72]. When ***Re*(nHo)$_2$** is dissolved in a non-protic solvent with a low polarity like ACN, the only evident emission band is the one attributed to an intraligand excited state, IL_{nHo}, where the emission spectrum of the complex is quite similar to the emission spectrum of the non-coordinated nHo ligand, with no spectral contributions at wavelength larger than 450 nm. On the contrary, emission spectrum of ***Re*(nHo)$_2$** recorded in methanolic solution (Fig. 5, left) shows two broad bands. The highest energy bands (λ ~ 360 – 390 nm) are attributed to the radiative decay of IL_{nHo} electronic states [68,73,74]. The emission centered at λ ~ 440 nm, has been previously attributed to an IL_{nHo} excited state where the n electrons of the pyridinic N are compromised, as in the cationic form of nHo ($nHoH^+$) [67,72]. In addition, a shoulder spans the 480 – 600 nm region of the spectra. As it was previously established, when an organic molecule is part of a transition metal complex, nonbonding electrons of the N atoms of the ligands, that contributed the nπ* excited state, is turned into a charge transfer (CT) excited state. Bearing this in mind we can assume that this effect could explain the similarities observed in the luminescence spectra in ACN and MeOH namely where interaction of solvent molecules with the nonbonding electrons is strong [53]. Conversely in DCM, the emission spectrum of non-coordinated nHo does not resemble the spectra of the complex. While the nHo emission band (IL_{nHo} excited state) is located at λ_{max} = 380 nm, a band centered at λ_{max} = 450 nm was

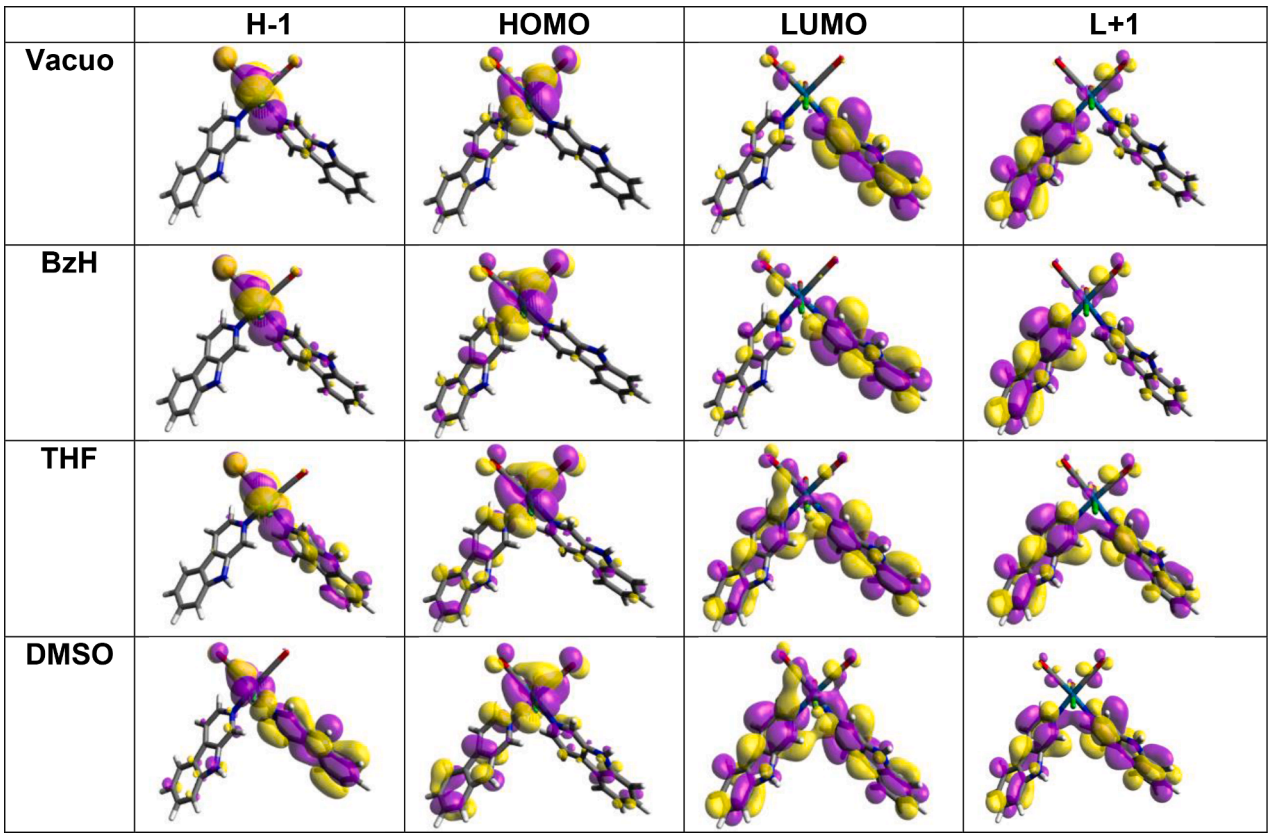

Fig. 3. Spatial plots of most representative MOs of ***Re*(nHo)$_2$** (isovalue = 0.02).

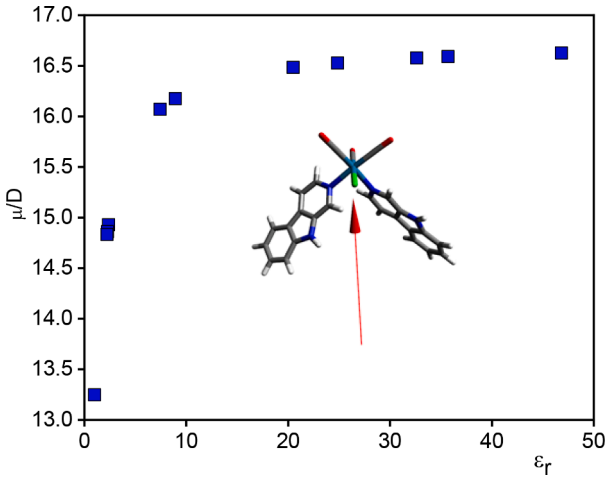

Fig. 4. Molecular dipole moment, μ, of ***Re*(nHo)$_2$** as a function of the dielectric constant, ε_r.

observed to ***Re*(nHo)$_2$**. Under acidic conditions, when the *n* electrons of the pyridinic N of the free nHo are compromised, as in $nHoH^+$, a λ_{max} of 450 nm is observed. This equivalence between the spectra of the $nHoH^+$ and ***Re*(nHo)$_2$** in DCM suggests that in this solvent the complex experiments a charge distribution where an electronic deficiency over the nHo is obtained and therefore the spectral features of an IL_{nHo} electron-deficient excited state is observed. In this sense, the nature of the excited state responsible for the luminescence at $\lambda \sim 450$ nm could be attributed to a protonated-like IL_{nHo} excited state [67]. The changes in the electronic density, along with the "*heavy atom effect*" caused by the *Re* atom can lead to an electronic distribution like the free $nHoH^+$, giving as a result similar emission spectral features.

Photoluminescence quantum yields (Φ_F), as well as the photoluminescence excited state lifetimes (τ) of ***Re*(nHo)$_2$**, were measured in ACN, DCM, and MeOH, and the results are depicted in Table 2. Luminescence lifetime were recorded at different wavelengths, depending on the prominent emission bands of the complex.

As shown in Table 2, both Φ_F and τ also depend in a certain way on the solvent. From the obtained values of τ, two main points can be discussed. First, as depicted, there is a mild dependency on the presence of O_2, as expected for this kind of compounds and their ability to interact with $^3O_2$ to generate $^1O_2$, (see below). Second, the obtained values for the two main IL_{nHo} emission bands closely resemble the τ previously reported for the excited states of non-coordinated nHo molecule [53, 67]. This outcome suggests once more, that the main emitting excited states in ***Re*(nHo)$_2$** are mainly IL_{nHo}.

3.3.2. *Photochemical reactions induced by laser flash photolysis (LFP)*

LFP measurements were carried out using a XeF laser ($\lambda_{ex} = 351$ nm). Fig. 6 shows the transient spectra obtained when either ***Re*(nHo)$_2$** or non-coordinated nHo solutions (10^{-5} M) were flash photolyzed in MeOH. As it can be observed, the main transient absorption band observed with ***Re*(nHo)$_2$** solution is centered at $\lambda_{max} \sim 555$ nm (blue). However, the main absorption band with the nHo solution is centered at $\lambda_{max} \sim 500$ nm (red). The latter spectral feature was previously attributed to an excited state of the nHo [68]. The spectra obtained are dissimilar and, therefore, the transient of ***Re*(nHo)$_2$** should not be assigned to an intrinsic IL_{nHo} excited state.

Besides, the decay of the transient of the complex after the irradiation adjusts perfectly to a monoexponential decay ($\tau = 75$ ns), suggesting that only one species is present. This lifetime is much longer than the luminescence lifetime of ***Re*(nHo)$_2$** (Table 2), and is markedly shorter than the reported (and also measured in this work) for the transient decay of non-coordinated nHo ($\tau = 2$ μs), as it is shown in the supplementary information (Figure S3) [53,68,72]. These differences

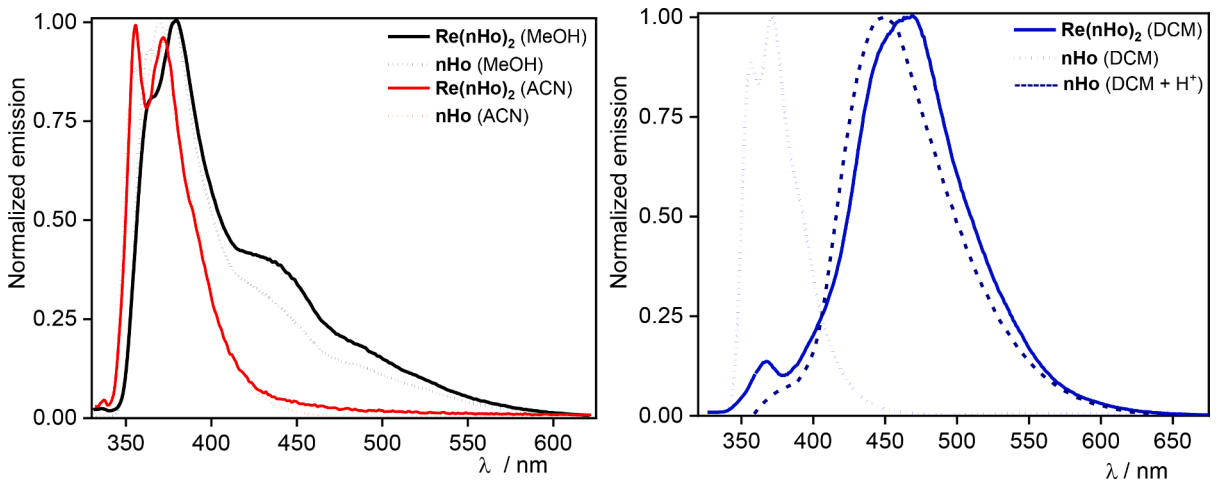

Fig. 5. Left: normalized emission spectra of ***Re*(nHo)$_2$** (dash lines) and nHo (dotted lines) in ACN (red) and MeOH (black). Right: normalized emission spectra of ***Re*(nHo)$_2$**, nHo in DCM and nHo in DCM + H^+ (dotted line and dashed line, respectively) λ_{ex} = 320 nm. Emission spectra of non-coordinated nHo are in agreement with that reported in the literature [53,68,71].

Table 2
Photoluminescence excited state lifetimes and emission quantum yields of ***Re*(nHo)$_2$** in different solvents.

Solvent	Φ_F	τ *Re*(nHo)$_2$ λ_{em} = 380 nm/air equilibrated/ns	τ *Re*(nHo)$_2$ λ_{em} = 380 nm/N_2 equilibrated/ns	τ *Re*(nHo)$_2$ λ_{em} = 450 nm/air equilibrated/ns	τ *Re*(nHo)$_2$ λ_{em} = 450 nm/N_2 equilibrated/ns
ACN	0.010	τ = 3.06 ± 0.02	τ = 3.84 ± 0.02	–	–
DCM	0.025	τ = 2.56 ± 0.02	τ = 2.71 ± 0.02	τ_1 = 1.25 ± 0.03 (93%) τ_2 = 20.4 ± 0.3 (7%)	τ_1 = 1.41 ± 0.06 (81%) τ_2 = 17.2 ± 0.2 (19%)
MeOH	0.018	τ = 3.77 ± 0.01	τ = 4.51 ± 0.02	τ_1 = 3.65 ± 0.04 (76%) τ_2 = 18.5 ± 0.1 (24%)	τ_1 = 4.36 ± 0.06 (72%) τ_2 = 26.2 ± 0.1 (28%)

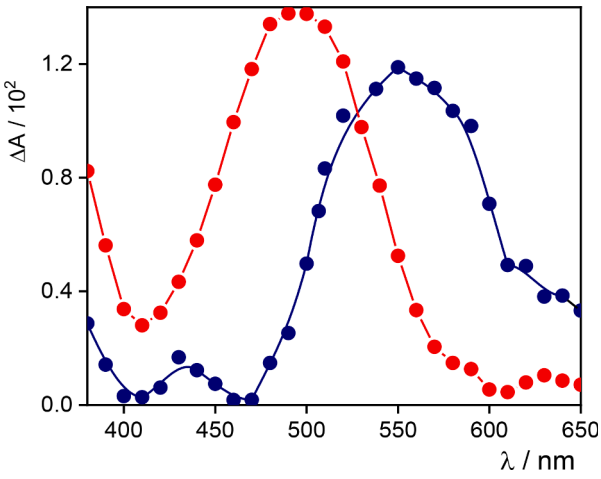

Fig. 6. LFP spectra for non-coordinated nHo (red) and ***Re*(nHo)$_2$** complex (blue) recorded in MeOH.

are explained by assuming that some excited states in the ***Re*(nHo)$_2$** complex are different than those present in the non-coordinated nHo, as observed previously in different coordination complexes with nHo as ligand [29].

The ability of the excited states to participate in redox reactions it is well documented in the literature [29,56,75,76]. The electron transfer reactions between the excited states of *Re*(I) complexes with the sacrificial electron donor triethylamine (TEA) as well as with the electron acceptor methyl viologen (MV^{+2}) are often used to probe their redox reactivity. Reductive quenching with amines, in particular, it is used for the identification of MLCT excited states. They react generating a reduced radical of complex. In this work, the ***Re*(nHo)$_2$** complex was flash irradiated in a neat MeOH solution (10^{-5} M) containing also 0.1 M TEA. The transient spectrum recorded is shown in Fig. 7.

This transient spectrum is very similar to the one observed in the absence of TEA Fig. 6). In addition, the decay lifetime of the transient observed was longer lived (τ = 6.04 μs) than excited state decay. These results suggest that the similarity between the excited state and the transient in Fig. 7 spectral features is the result of the charge separation established in the complex when an excited state $MLCT_{Re\rightarrow nHo}$ is populated (formally *Re*(II) and a ligand radical anion) and the net location of an electron in the ligand, i.e., forming the reduced radical generated by reaction of the MLCT with TEA, Eq. (4) and ((5).

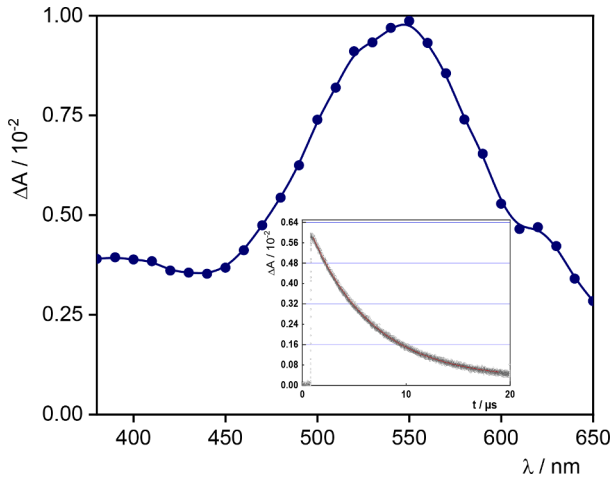

Fig. 7. LFP spectra of ***Re*(nHo)$_2$** with an excess of TEA in MeOH (λ_{ex} = 351 nm). *Inset*: oscillographic trace recorded at λ_{ob} = 550 nm showing the decay of the transient absorbance (ΔA), with a lifetime τ = 6.04 μs.

$$\left[\mathrm{ClRe^{I}(CO)_3(nHo)_2}\right] \xrightarrow{h\nu} \left[\mathrm{ClRe^{II}(CO)_3(nHo)(nHo^{\bullet -})}\right]^{*} \quad (4)$$

$$\left[\mathrm{ClRe^{II}(CO)_3(nHo)(nHo^{\bullet -})}\right]^{*} \xrightarrow[-\mathrm{TEA}^{\bullet +}]{+\mathrm{TEA}} \left[\mathrm{ClRe^{I}(CO)_3(nHo)(nHo^{\bullet -})}\right] \quad (5)$$

Thus, contrasting what is observed in a non-coordinated nHo solution, an MLCT excited state is generated when a solution of ***Re*(nHo)$_2$** was flash photolyzed.

3.3.3. Pulse radiolysis (PR)

The pulse radiolysis technique was used also to generate the reduced radical of ***Re*(nHo)$_2$** complex by reaction mainly with solvated electrons, e^{-}_{solv}, (experimental conditions MeOH/N_2, see 2.4 section).

Fig. 8 shows that the spectrum for the reduced species of ***Re*(nHo)$_2$**, (blue), consist of a narrow band at λ ~ 390 nm along with a broad band at λ ~ 550 nm, both bands nearly with the same intensity. The same spectral features are observed in the reduction of non-coordinated nHo (red). Hence, the complex is reduced by the thermal reaction with e^{-}_{solv} producing a radical, eq. (6).

$$\left[\mathrm{ClRe^{I}(CO)_3(nHo)_2}\right] \xrightarrow{e^{-}_{solv}} \left[\mathrm{ClRe^{I}(CO)_3(nHo)(nHo^{\bullet -})}\right] \quad (6)$$

The high spectral resemblance between the spectrum generated by PR and the spectrum recorded by LFP in the reductive quenching with TEA (Fig. 7), confirms the ***Re*(nHo)$_2$** role of electron acceptor in the photoinduced process in which the participation of a $\mathrm{MLCT_{Re\rightarrow nHo}}$ excited state must be required [29].

Oxidative quenching of ***Re*(nHo)$_2$** was investigated by the LFP generation of the excited states of the complex in the presence of MV^{+2}. The latter species oxidize the excited state of the complex producing the radical $MV^{\bullet +}$. Such a radical exhibits a characteristic absorption at λ ~ 600 nm (Figure S4). The redox process must involve the photogeneration of MLCT, eq. (4), followed by its reaction with MV^{+2}, eq. (7).

$$\left[\mathrm{ClRe^{II}(CO)_3(nHo)(nHo^{\bullet -})}\right]^{*} + \mathrm{MV^{+2}} \rightarrow \left[\mathrm{ClRe^{II}(CO)_3(nHo)_2}\right]^{+} + \mathrm{MV^{\bullet +}} \quad (7)$$

Solutions of the complex with MV^{+2} were flash irradiated at 351 nm. The rate constants of the quenching reactions were determined by varying the concentration of MV^{+2} while keeping the complex concentration constant. The kinetics of the reactions was investigated under a pseudo-first-order regime in MV^{+2} concentration. A single exponential decay of the excited state with a rate constant (k_d), eq. (8), corresponding to a pseudo-first-order dependence on MV^{+2} concentration was obtained [29,76].

$$\Delta A_t = \Delta A_0 e^{-k_d t} \quad (8)$$

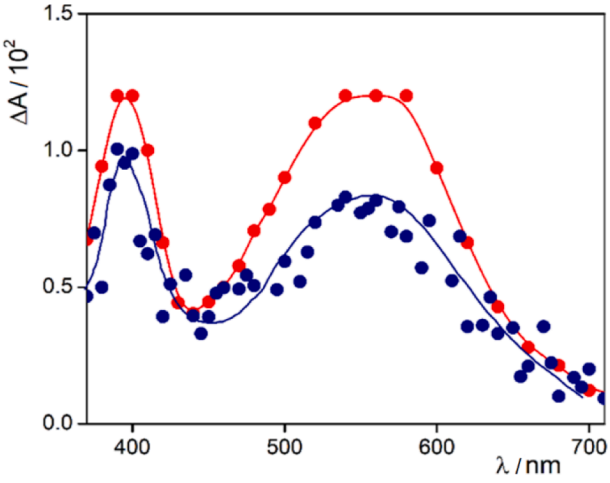

Fig. 8. Pulse radiolysis spectra of ***Re*(nHo)$_2$** (blue) and non-coordinated nHo (red) of N_2 deaerated solutions (10^{-5} M, MeOH).

The quenching rate constant (k_q) was calculated from the slope of the plot k_d vs MV^{+2}, yielding the value $k_q = 4.8 \times 10^9\ M^{-1}s^{-1}$ (Fig. 9). This value of k_q is in within the order of magnitude of k_q constants in the literature for structurally related complexes [29,77,78]. Furthermore, it is 2.3 to 34.3 times greater than those reported for the relative complexes $[(nHo)Re(CO)_3(L)]^{+}$, where L = bidentate N,N-ligands [29]. In sum, the excited state oxidation reaction of ***Re*(nHo)$_2$** occurs with greater ease than those complexes with bidentate ligands. Such a greater ease is probably due to steric effects that energetically optimize the reaction path for monodentate ligands.

3.3.4. Singlet oxygen generation and optoacoustic measurements

Singlet oxygen generation by the ***Re*(nHo)$_2$** complex in ACN solutions was analyzed by time-resolved phosphorescence measurements (1270 nm). The phosphorescence showed clear evidence of singlet oxygen formation. Linear correlations were obtained from the plots of the dependence of the singlet oxygen phosphorescence intensity emission at zero time, S(0), as a function of the laser energy for the complex and the reference. From these slopes (Figure S5) and the usual procedure described elsewhere [62,79], the determined quantum yield of singlet oxygen production was $\Phi\Delta = 0.25 \pm 0.02$. This result is similar to values of ΦΔ of *Re*(I) complexes which have similar structures or with nHo as ligand [30,62,80].

As observed in Fig. 10, the photoacoustic signal of ***Re*(nHo)$_2$,** as well as the reference in ACN solutions, showed the same behavior: no time shift or changes of shape, with respect to the calorimetric reference signal (inset of Fig. 10). Linear relationships in both solvents were obtained between the amplitude of the first optoacoustic signal (H) and the excitation fluence (F) for samples and references at various A, in a fluence range between 1 and 10 J/m^2. The ratio between the slopes of these lines for sample and reference yielded the values of α for the samples. From these plots, considering that $a_R = 1$ for CR, the a value = 0.89 ± 0.04 was obtained for ***Re*(nHo)$_2$** complex. Consequently, this complex released to the medium almost all the absorbed energy as prompt heat (integrated by the transducer) in processes faster than $\tau_R/5$. These values, combined with the photochemical data, were satisfactorily adjusted to the energy balance [62,66], where the molar exciting energy from the laser photon (E_λ = 80.5 kcal/mol at 355 nm) provides the sum of the fraction of energy dissipated as prompt heat, plus the energy lost in rapid radiative processes, e.g. fluorescence, and the energy "stored" in long-lived transient species, such as a singlet oxygen.

4. Conclusions

The photophysical and photochemical properties of ClRe$(CO)_3(nHo)_2$ were studied in solution phase. These results allowed us to

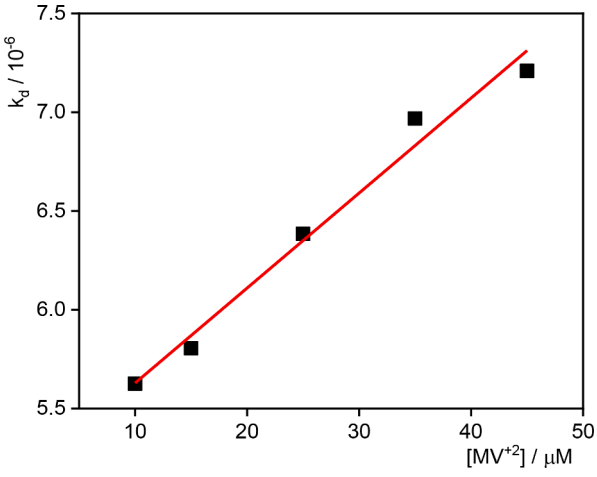

Fig. 9. Plot of k_d vs $[MV^{+2}]$. k_q is represented as the slope of the linear fit.

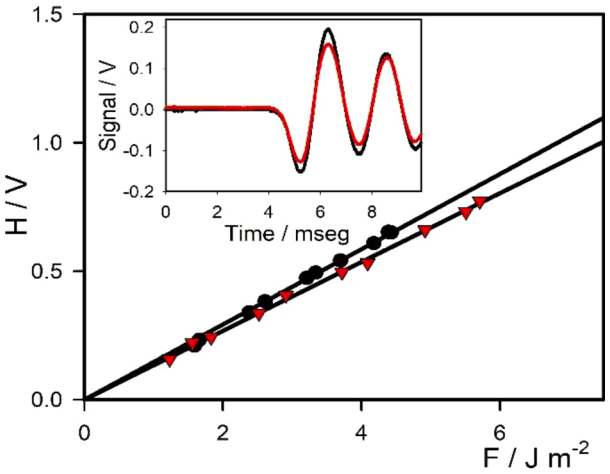

Fig. 10. Amplitude of the photoacoustic signals as a function of laser fluence for ACN solutions: 2-Hydroxybenzophenone (2-HBP, •), ***Re*(nHo)$_2$** complex (▼). *Inset*: Normalized photoacoustic signals of ACN solutions for 2-HBP (black line) and the ***Re*(nHo)$_2$** complex (red line) with matched absorbances (0.158 ± 0.002).

identify and study the reactivity of the β-carboline Rhenium(I) complex main excited states. The absorption spectrum as well as the steady-state and time-resolved luminescence of ***Re*(nHo)$_2$** complex exhibits a marked dependence with the solvent properties. TD-DFT calculations established that the most important electronic transitions present in the low energy region of the spectrum in all solvents are $MLLCT_{Re(CO)3\rightarrow nHo1, nHo2}$ along with a mixture of IL_{nHo} and $LLCT_{Cl\rightarrow nHo}$ transitions. The magnitude of the calculated dipole moment increases when the polarity of the solvent is increased. The latter was established due the electron density inside the complex becomes more diffuse and is enhanced outside the molecular limits. The complex luminescence is mainly attributed to the emitting $^1IL_{nHo}$ state although overlapping emission from ^{3}MLCT states in the low energy region cannot be ruled out. However, in flash photolysis experiments the MLCT excited states generated govern the photochemistry of the complex. The excited state of ***Re*(nHo)$_2$** complex can efficiently generate singlet oxygen as well as reduced radicals or oxidized species of *Re*(II) reactive against substrates present, for example, in cellular environments. These photophysical properties suggest the potential application of ***Re*(nHo)$_2$** complex in photodynamic therapy (PDT) or photoactivated chemotherapy (PACT), antioxidant activity, or photocytotoxicity. In this sense, the cellular uptake characteristics of the ***Re*(nHo)$_2$** in A549 cells as well as their cytotoxicity against these human carcinoma lung cells, acquire even more relevance [25]. Moreover, after photonic excitation, almost all the absorbed energy by the complex is released to the medium as prompt heat. This thermal feature could be of interest also for new alternative therapies such as regional hyperthermia that allows counteracting tumor growth and progression due to a localized increase of the temperature inside of the cancer cell. The photophysical properties established in the $ClRe(CO)_3(nHo)_2$ allow us to imagine some intracellular photobiological action that could be modulated by the difference in the polarity of the different cell compartments.

Declaration of Competing Interest

The authors declare that they have no known competing financial interests or personal relationships that could have appeared to influence the work reported in this paper.

Acknowledgments

This work was supported in part by CONICET (PIP 112–2013–01–00236CO), ANPCyT (PICT 2018–03193 and PICT 2018–03341) and UNLP (11/X779 and 11/X679) Argentina. F.M.C, E. W. and G.T.R. are Research Members of CONICET (Argentina). P.D.G. is a Research Member of CICBA (Argentina). I.M. thanks ANPCyT, CONICET and the Fulbright Program for research scholarships. Part of this work was also carried out in the Notre Dame Radiation Laboratory (NDRL). The NDRL is supported by the Division of Chemical Sciences, Geosciences and Biosciences, Basic Energy Sciences, Office of Science, United States Department of Energy through grant number DE-FC02–04ER15533. This is contribution number NDRL 5320.

Supplementary materials

Supplementary material associated with this article can be found, in the online version, at doi:10.1016/j.jpap.2021.100078.

References

[1] J.R.F. Allen, B.R. Holmstedt, The simple β-carboline alkaloids, Phytochemistry 19 (1980) 1573–1582, https://doi.org/10.1016/S0031-9422(00)83773-5.
[2] K. Pari, C.S. Sundari, S. Chandani, D. Balasubramanian, β-Carbolines that accumulate in human tissues may serve a protective role against oxidative stress, J. Biol. Chem. 275 (2000) 2455–2462, https://doi.org/10.1074/jbc.275.4.2455.
[3] J. Adachi, Y. Mizoi, T. Naito, Y. Ogawa, Y. Uetani, I. Ninomiya, Identification of Tetrahydro-β-carboline-3-carboxylic acid in foodstuffs, human urine and human Milk, J. Nutr. 121 (1991) 646–652, https://doi.org/10.1093/jn/121.5.646.
[4] K. Suzuki, I. Nomura, M. Ninomiya, K. Tanaka, M. Koketsu, Synthesis and antimicrobial activity of β-carboline derivatives with N^2-alkyl modifications, Bioorg. Med. Chem. Lett. 28 (2018) 2976–2978, https://doi.org/10.1016/j.bmcl.2018.06.050.
[5] G. Nenaah, Antibacterial and antifungal activities of (beta)-carboline alkaloids of Peganum harmala (L) seeds and their combination effects, Fitoterapia 81 (2010) 779–782, https://doi.org/10.1016/j.fitote.2010.04.004.
[6] D.J. Moura, M.F. Richter, J.M. Boeira, J.A. Pegas Henriques, J. Saffi, Antioxidant properties of beta-carboline alkaloids are related to their antimutagenic and antigenotoxic activities, Mutagenesis 22 (2007) 293–302, https://doi.org/10.1093/mutage/gem016.
[7] M.M. Gonzalez, F.M. Cabrerizo, A. Baiker, R. Erra-Balsells, A. Osterman, H. Nitschko, M.G. Vizoso-Pinto, β-Carboline derivatives as novel antivirals for herpes simplex virus, Int. J. Antimicrob. Agents. 52 (2018) 459–468, https://doi.org/10.1016/j.ijantimicag.2018.06.019.
[8] V.M. Quintana, L.E. Piccini, J.D. Panozzo Zénere, E.B. Damonte, M.A. Ponce, V. Castilla, Antiviral activity of natural and synthetic β-carbolines against dengue virus, Antiviral Res 134 (2016) 26–33, https://doi.org/10.1016/j.antiviral.2016.08.018.
[9] M.L. Alomar, F.A. Rasse-Suriani, A. Ganuza, V.M. Cóceres, F.M. Cabrerizo, S. O. Angel, In vitro evaluation of β-carboline alkaloids as potential anti-Toxoplasma agents, BMC Res. Notes. 6 (2013) 193, https://doi.org/10.1186/1756-0500-6-193.
[10] G.M. Olmedo, L. Cerioni, M.M. González, F.M. Cabrerizo, V.A. Rapisarda, S. I. Volentini, Antifungal activity of β-carbolines on *Penicillium digitatum* and Botrytis cinerea, Food Microbiol 62 (2017) 9–14, https://doi.org/10.1016/j.fm.2016.09.011.
[11] M.M. Gonzalez, M. Vignoni, M. Pellon-Maison, M.A. Ales-Gandolfo, M.R. Gonzalez-Baro, R. Erra-Balsells, B. Epe, F.M. Cabrerizo, Photosensitization of DNA by β-carbolines: kinetic analysis and photoproduct characterization, Org. Biomol. Chem. 10 (2012) 1807, https://doi.org/10.1039/c2ob06505c.
[12] R.K. Downum, Light-activated plant defence, 1992.
[13] G.M. Olmedo, L. Cerioni, M.M. González, F.M. Cabrerizo, S.I. Volentini, V. A. Rapisarda, UVA Photoactivation of Harmol enhances its antifungal activity against the phytopathogens *Penicillium digitatum* and *Botrytis cinerea*, Front. Microbiol. 8 (2017), https://doi.org/10.3389/fmicb.2017.00347.
[14] M.P. Denofrio, F.A.O. Rasse-Suriani, J.M. Paredes, F. Fassetta, L. Crovetto, M. D. Giron, R. Salto, B. Epe, F.M. Cabrerizo, N-Methyl-β-carboline alkaloids: structure- dependent photosensitizing properties and localization in subcellular domains, Org. Biomol. Chem. Advance Ar (2020), https://doi.org/10.1515/ci.2004.26.6.31.
[15] K. Butzbach, F.A.O. Rasse-Suriani, M.M. Gonzalez, F.M. Cabrerizo, B. Epe, Albumin-folate conjugates for drug-targeting in photodynamic therapy, Photochem. Photobiol. 92 (2016) 611–619, https://doi.org/10.1111/php.12602.
[16] M. Vignoni, R. Erra-Balsells, B. Epe, F.M. Cabrerizo, Intra- and extra-cellular DNA damage by harmine and 9-methyl-harmine, J. Photochem. Photobiol. B Biol. 132 (2014) 66–71, https://doi.org/10.1016/j.jphotobiol.2014.01.020.
[17] J.G. Yañuk, M.P. Denofrio, F.A.O. Rasse-Suriani, F.D. Villarruel, F. Fassetta, F. S. García Einschlag, R. Erra-Balsells, B. Epe, F.M. Cabrerizo, DNA damage photo-induced by chloroharmine isomers: hydrolysis: versus oxidation of nucleobases, Org. Biomol. Chem. 16 (2018) 2170–2184, https://doi.org/10.1039/c8ob00162f.
[18] F. Ragone, G.T. Ruiz, O.E. Piro, G.A. Echeverría, F.M. Cabrerizo, G. Petroselli, R. Erra-Balsells, K. Hiraoka, F.S. García Einschlag, E. Wolcan, Water-Soluble (Pterin)rhenium(I) complex: synthesis, structural characterization, and two reversible protonation-deprotonation behavior in aqueous solutions, Eur. J. Inorg. Chem. 2012 (2012) 4801–4810, https://doi.org/10.1002/ejic.201200681.

[19] V. Fernández-Moreira, M.L. Ortego, C.F. Williams, M.P. Coogan, M.D. Villacampa, M.C. Gimeno, Bioconjugated Rhenium(I) complexes with amino acid derivatives: synthesis, photophysical properties, and cell imaging studies, Organometallics 31 (2012) 5950–5957, https://doi.org/10.1021/om300610j.

[20] A.V. Shtemenko, P. Collery, N.I. Shtemenko, K.V. Domasevitch, E.D. Zabitskaya, A. A. Golichenko, Synthesis, characterization, in vivo antitumor properties of the cluster rhenium compound with GABA ligands and its synergism with cisplatin, Dalton Trans (2009) 5132, https://doi.org/10.1039/b821041a.

[21] M. Muñoz-Osses, F. Godoy, A. Fierro, A. Gómez, N. Metzler-Nolte, New organometallic imines of rhenium(I) as potential ligands of GSK-3β: synthesis, characterization and biological studies, Dalton Trans 47 (2018) 1233–1242, https://doi.org/10.1039/C7DT04344A.

[22] S. Kunze, F. Zobi, P. Kurz, B. Spingler, R. Alberto, Vitamin B12 as a ligand for technetium and rhenium complexes, Angew. Chemie Int. Ed. 43 (2004) 5025–5029, https://doi.org/10.1002/anie.200460923.

[23] Y.O. Ayipo, W.A. Osunniran, M.N. Mordi, Metal complexes of β-carboline: advances in anticancer therapeutics, Coord. Chem. Rev. 432 (2021), 213746, https://doi.org/10.1016/j.ccr.2020.213746.

[24] L. He, Z.-.Y. Pan, W.-.W. Qin, Y. Li, C.-.P. Tan, Z.-.W. Mao, Impairment of the autophagy-related lysosomal degradation pathway by an anticancer rhenium(I) complex, Dalton Trans 48 (2019) 4398–4404, https://doi.org/10.1039/C9DT00322C.

[25] I. Maisuls, E. Wolcan, O.E. Piro, E.E. Castellano, G. Petroselli, R. Erra-Balsells, F. M. Cabrerizo, G.T. Ruiz, Synthesis, structural characterization and biological evaluation of Rhenium(I) Tricarbonyl complexes with β-Carboline ligands, ChemistrySelect 2 (2017) 8666–8672, https://doi.org/10.1002/slct.201701961.

[26] I. Maisuls, E. Wolcan, O.E. Piro, G.A. Etcheverría, G. Petroselli, R. Erra-Ballsels, F. M. Cabrerizo, G.T. Ruiz, Norharmane rhenium(I) polypyridyl complexes: synthesis, structural and spectroscopic characterization, Dalton Trans 44 (2015) 17064–17074, https://doi.org/10.1039/C5DT02790J.

[27] C. Tan, S. Lai, S. Wu, S. Hu, L. Zhou, Y. Chen, M. Wang, Y. Zhu, W. Lian, W. Peng, L. Ji, A. Xu, Nuclear Permeable Ruthenium(II) β-Carboline complexes induce autophagy to antagonize mitochondrial-mediated apoptosis, J. Med. Chem. 53 (2010) 7613–7624, https://doi.org/10.1021/jm1009296.

[28] L. He, S.-.Y. Liao, C.-.P. Tan, Y.-.Y. Lu, C.-.X. Xu, L.-.N. Ji, Z.-.W. Mao, Cyclometalated iridium(iii)–β-carboline complexes as potent autophagy-inducing agents, Chem. Commun. 50 (2014) 5611, https://doi.org/10.1039/c4cc01461h.

[29] I. Maisuls, F.M. Cabrerizo, A.G. Lappin, G.T. Ruiz, G.J. Ferraudi, Photophysical properties of $[(norharmane)Re(CO)_3(L)]^+$ complexes (L = bpy, phen or dppz). Redox behavior of the excited states and their interaction with Calf Thymus DNA, J. Photochem. Photobiol. A Chem. 364 (2018) 169–176, https://doi.org/10.1016/j.jphotochem.2018.05.007.

[30] I. Maisuls, F.M. Cabrerizo, P.M. David-Gara, B. Epe, G.T. Ruiz, DNA Oxidation Photoinduced by Norharmane Rhenium(I) Polypyridyl Complexes: effect of the Bidentate N,N′-ligands on the damage profile, Chem. - A Eur. J. 24 (2018) 12902–12911, https://doi.org/10.1002/chem.201801272.

[31] K.K.-W. Lo, Exploitation of luminescent organometallic Rhenium(I) and Iridium (III) complexes in biological studies, in: 2010: pp. 73–114. https://doi.org/10.1007/3418_2009_3.

[32] A. Kumar, S.-.S. Sun, A.J. Lees, Photophysics of Organometallics, Berlin and Heidelberg, Germany, 2010.

[33] H. Takeda, K. Koike, T. Morimoto, H. Inumaru, O. Ishitani, Photochemistry and photocatalysis of rhenium(I) diimine complexes, in: 2011: pp. 137–186. https://doi.org/10.1016/B978-0-12-385904-4.00007-X.

[34] I. Maisuls, S. Ostendorp, G. Wilde, A.J. Parola, C.A. Strassert, E. Wolcan, Energy transfer between CNT surface and $-Re(CO)_3(phen)^{+}$* Pendants Grafted to P4VP in Nanohybrid Shish-Kebob-like Structures, J. Phys. Chem. C. 3 (2020), https://doi.org/10.1021/acs.jpcc.9b10567.

[35] H.H. Martinez Saavedra, F. Ragone, G.T. Ruiz, P.M.D. Gara, E. Wolcan, Solvent dependent switching of ^{3}MLLCT and ^{1}IL luminescent states in $[ClRe(CO)_3(Bathocuproinedisulfonate)]_2^{-}$: spectroscopic and computational study, J. Phys. Chem. A. 118 (2014) 9661–9674, https://doi.org/10.1021/jp506890r.

[36] L. Wei, J.W. Babich, W. Ouellette, J. Zubieta, Developing the $\{M(CO)_3\}^+$ core for fluorescence applications: rhenium Tricarbonyl core complexes with benzimidazole, quinoline, and tryptophan derivatives, Inorg. Chem. 45 (2006) 3057–3066, https://doi.org/10.1021/ic0517319.

[37] D.J. Stufkens, The remarkable properties of α-Diimine Rhenium Tricarbonyl complexes in their Metal-to-Ligand Charge-Transfer (MLCT) excited states, Comments Inorg. Chem. 13 (1992) 359–385, https://doi.org/10.1080/02603599208048467.

[38] B.S. Uppal, R.K. Booth, N. Ali, C. Lockwood, C.R. Rice, P.I.P. Elliott, Synthesis and characterisation of luminescent rhenium tricarbonyl complexes with axially coordinated 1,2,3-triazole ligands, Dalton Trans 40 (2011) 7610–7616, https://doi.org/10.1039/c1dt10634a.

[39] K.K.-W. Lo, K.Y. Zhang, S.P.-Y. Li, Recent Exploitation of Luminescent Rhenium(I) Tricarbonyl Polypyridine Complexes as Biomolecular and Cellular Probes, Eur. J. Inorg. Chem. 2011 (2011) 3551–3568, https://doi.org/10.1002/ejic.201100469.

[40] S. Sato, O. Ishitani, Photochemical reactions of *fac*-rhenium(I) tricarbonyl complexes and their application for synthesis, Coord. Chem. Rev. 282–283 (2015) 50–59, https://doi.org/10.1016/j.ccr.2014.05.009.

[41] L.L.B. Bracco, R.O. Lezna, J. Muñoz-Zuñiga, G.T. Ruiz, M.R. Féliz, G.J. Ferraudi, F. S. García Einschlag, E. Wolcan, On the mechanism of formation and spectral properties of radical anions generated by the reduction of $-[Re^I(CO)_3(5\text{-}nitro\text{-}1,10\text{-}phenanthroline)]^+$ and $-[Re^I(CO)_3(3,4,7,8\text{-}tetramethyl\text{-}1,10\text{-}phenanthroline)]$, Inorganica Chim. Acta. 370 (2011) 482–491, https://doi.org/10.1016/j.ica.2011.02.039.

[42] M.P. Juliarena, R.O. Lezna, G.T. Ruiz, M.R. Féliz, G.J. Ferraudi, E. Wolcan, On the nature of the redox products of $4\text{-}((CH_3)_2N)C_6H_4\text{–}CO_2-$ and $4\text{-}((CH_3)_2N)C_6H_4\text{–}CO_2\text{–}Re(CO)_3$(1,10-phenanthroline): a spectroelectrochemical, pulse radiolysis and flash photochemical study, Polyhedron 27 (2008) 1471–1478, https://doi.org/10.1016/j.poly.2008.01.006.

[43] G.T. Ruiz, M.P. Juliarena, E. Wolcan, G. Ferraudi, Kinetic and spectroscopic observations on the azidyl,, radical oxidation of $fac\text{-}(L_{spectator})Re^I(CO)_3(L_{acceptor})$ to $fac\text{-}(L_{spectator})Re^{II}(CO)_3(L_{acceptor})$, $L_{spectator}$=4,4′-bpy; $L_{acceptor}$=dipyridyl[3,2-*a*:2′3′-*c*]phenazine or $L_{spectator}=Cl^-$; $L_{acceptor}$=bathocup, Inorganica Chim. Acta 360 (2007) 3681–3687, https://doi.org/10.1016/j.ica.2007.02.049.

[44] E.B. Bauer, A.A. Haase, R.M. Reich, D.C. Crans, F.E. Kühn, Organometallic and coordination rhenium compounds and their potential in cancer therapy, Coord. Chem. Rev. 393 (2019) 79–117, https://doi.org/10.1016/j.ccr.2019.04.014.

[45] A. Leonidova, G. Gasser, Underestimated potential of organometallic rhenium complexes as anticancer agents, ACS Chem. Biol. 9 (2014) 2180–2193, https://doi.org/10.1021/cb500528c.

[46] F.L. Thorp-Greenwood, J.A. Platts, M.P. Coogan, Experimental and theoretical characterisation of phosphorescence from rhenium polypyridyl tricarbonyl complexes, Polyhedron 67 (2014) 505–512, https://doi.org/10.1016/j.poly.2013.09.033.

[47] R.G. Balasingham, M.P. Coogan, F.L. Thorp-Greenwood, Complexes in context: attempting to control the cellular uptake and localisation of rhenium *fac*-tricarbonyl polypyridyl complexes, Dalton Trans 40 (2011) 11663, https://doi.org/10.1039/c1dt11219h.

[48] V. Fernández-Moreira, F.L. Thorp-Greenwood, A.J. Amoroso, J. Cable, J.B. Court, V. Gray, A.J. Hayes, R.L. Jenkins, B.M. Kariuki, D. Lloyd, C.O. Millet, C.F. Williams, M.P. Coogan, Uptake and localisation of rhenium *fac*-tricarbonyl polypyridyls in fluorescent cell imaging experiments, Org. Biomol. Chem. 8 (2010) 3888, https://doi.org/10.1039/c004610h.

[49] A.J. Amoroso, M.P. Coogan, J.E. Dunne, V. Fernández-Moreira, J.B. Hess, A. J. Hayes, D. Lloyd, C. Millet, S.J.A. Pope, C. Williams, Rhenium *fac*-tricarbonyl bisimine complexes: biologically useful fluorochromes for cell imaging applications, Chem. Commun. (2007) 3066–3068, https://doi.org/10.1039/B706657K.

[50] P. Collery, D. Desmaele, V. Vijaykumar, Design of Rhenium compounds in targeted anticancer therapeutics, Curr. Pharm. Des. 25 (2019) 3306–3322, https://doi.org/10.2174/1381612825666190902161400.

[51] L. He, Z.-.Y. Pan, W.-.W. Qin, Y. Li, C.-.P. Tan, Z.-.W. Mao, Impairment of the autophagy-related lysosomal degradation pathway by an anticancer rhenium^I complex, Dalton Trans 48 (2019) 4398–4404, https://doi.org/10.1039/C9DT00322C.

[52] T.W. Ebbesen, G. Ferraudi, Photochemistry of methyl viologen in aqueous and methanolic solutions, J. Phys. Chem. 87 (1983) 3717–3721, https://doi.org/10.1021/j100242a028.

[53] O.I. Tarzi, M.A. Ponce, F.M. Cabrerizo, S.M. Bonesi, R. Erra-Balsells, Electronic spectroscopy of the β-carboline derivatives nitronorharmanes, nitroharmanes, nitroharmines and chloroharmines in homogeneous media and in solid matrix, Arkivoc 2005 (2006) 295–310, https://doi.org/10.3998/ark.5550190.0006.c23.

[54] A. Pardo, D. Reyman, J.M.L. Poyato, F. Medina, Some β-carboline derivatives as fluorescence standards, J. Lumin. 51 (1992) 269–274, https://doi.org/10.1016/0022-2313(92)90077-M.

[55] K.P. Ghiggino, P.F. Skilton, P.J. Thistlethwaite, β-Carboline as a fluorescence standard, J. Photochem. 31 (1985) 113–121, https://doi.org/10.1016/0047-2670(85)85079-6.

[56] A.S. Moncada, F.S.G. Einschlag, E.D. Prieto, G.T. Ruiz, A.G. Lappin, G.J. Ferraudi, E. Wolcan, Photophysical properties of $Re^I(CO)_3$(phen) pendants grafted to a poly-4-vinylpyridine backbone. A correlation between photophysical properties and morphological changes of the backbone, J. Photochem. Photobiol. A Chem. 321 (2016) 284–296, https://doi.org/10.1016/j.jphotochem.2016.01.001.

[57] M. Sarakha, M. Cozzi, G. Ferraudi, Mechanism of (μ-H)(μ-alkenyl)$Re_2(CO)_8$ Formation in 350nm Flash Irradiations of $Re_2(CO)_{10}$, Inorg. Chem. 35 (1996) 3804–3807, https://doi.org/10.1021/ic951483o.

[58] G.V. Buxton, C.L. Greenstock, W.P. Helman, A.B. Ross, Critical Review of rate constants for reactions of hydrated electrons, hydrogen atoms and hydroxyl radicals (•OH/•O$^-$ in Aqueous Solution, J. Phys. Chem. Ref. Data. 17 (1988) 513–886, https://doi.org/10.1063/1.555805.

[59] G.L. Hug, Y. Wang, C. Schöneich, P.-.Y. Jiang, R.W. Fessenden, Multiple time scales in pulse radiolysis. Application to bromide solutions and dipeptides, Radiat. Phys. Chem. 54 (1999) 559–566, https://doi.org/10.1016/S0969-806X(98)00303-X.

[60] N. Getoff, A. Ritter, F. Schwörer, P. Bayer, Primary yields of CH_3•O and •CH_2OH radicals resulting in the radiolysis of high purity methanol, Radiat. Phys. Chem. 41 (1993) 797–801, https://doi.org/10.1016/0969-806X(93)90025-P.

[61] M. Simic, P. Neta, E. Hayon, Pulse radiolysis study of alcohols in aqueous solution, J. Phys. Chem. 73 (1969) 3794–3800, https://doi.org/10.1021/j100845a038.

[62] F. Ragone, H.H.M. Saavedra, P.M.D. Gara, G.T. Ruiz, E. Wolcan, Photosensitized Generation of Singlet Oxygen from *Re*(I) Complexes: a Photophysical Study Using LIOAS and Luminescence Techniques, J. Phys. Chem. A. 117 (2013) 4428–4435, https://doi.org/10.1021/jp402550g.

[63] R. Schmidt, C. Tanielian, R. Dunsbach, C. Wolff, Phenalenone, a universal reference compound for the determination of quantum yields of singlet oxygen $O_2(^1\Delta_g)$ sensitization, J. Photochem. Photobiol. A Chem. 79 (1994) 11–17, https://doi.org/10.1016/1010-6030(93)03746-4.

[64] P. Van Haver, L. Viaene, M. Van der Auweraer, F. De Schryver, References for laser-induced opto-acoustic spectroscopy using UV excitation, J. Photochem. Photobiol. A Chem. 63 (1992) 265–277, https://doi.org/10.1016/1010-6030(92)85192-W.

[65] S. Abbruzzetti, C. Viappiani, D.H. Murgida, R. Erra-Balsells, G.M. Bilmes, Non-toxic, water-soluble photocalorimetric reference compounds for UV and visible excitation, Chem. Phys. Lett. 304 (1999) 167–172, https://doi.org/10.1016/S0009-2614(99)00306-1.
[66] S.E. Braslavsky, G.E. Heibel, Time-resolved photothermal and photoacoustic methods applied to photoinduced processes in solution, Chem. Rev. 92 (1992) 1381–1410, https://doi.org/10.1021/cr00014a007.
[67] M.M. Gonzalez, M.L. Salum, Y. Gholipour, F.M. Cabrerizo, R. Erra-Balsells, Photochemistry of norharmane in aqueous solution, Photochem. Photobiol. Sci. 8 (2009) 1139, https://doi.org/10.1039/b822173a.
[68] R.S. Becker, L.F.V. Ferreira, F. Elisei, I. Machado, L. Latterini, Comprehensive Photochemistry and Photophysics of Land- and Marine-based β-carbolines Employing Time-resolved Emission and Flash Transient Spectroscopy, Photochem. Photobiol. 81 (2005) 1195, https://doi.org/10.1562/2005-03-22-RA-469.
[69] J.A. Riddick, W.B. Bunger, K.T. Sakano, Organic Solvents : Physical Properties and Methods of Purification, Wiley, New York, 1986.
[70] A. Kumar, S.-.S. Sun, A.J. Lees, Photophysics and Photochemistry of Organometallic Rhenium Diimine complexes, in: 2009: pp. 37–71. https://doi.org/10.1007/3418_2009_2.
[71] M.J. Tapia, D. Reyman, M.H. Viñas, C. Carcedo, J.J. Camacho, Hydrogen-bonding interactions of norharmane in mixtures of acetic acid with benzene, p-dioxane and acetonitrile, Phys. Chem. Chem. Phys. 4 (2002) 3676–3683, https://doi.org/10.1039/b201526a.
[72] M.Micaela Gonzalez, J. Arnbjerg, M.Paula Denofrio, R. Erra-Balsells, P.R. Ogilby, F. M. Cabrerizo, One- and two-photon excitation of β-carbolines in aqueous solution: ph-dependent spectroscopy, photochemistry, and photophysics, J. Phys. Chem. A. 113 (2009) 6648–6656, https://doi.org/10.1021/jp902105x.
[73] A. Dias, A.P. Varela, M. da G. Miguel, A.L. Macanita, R.S. Becker, β-Carboline photosensitizers. 1. Photophysics, kinetics and excited-state equilibria in organic solvents, and theoretical calculations, J. Phys. Chem. 96 (1992) 10290–10296, https://doi.org/10.1021/j100204a036.
[74] H.D. Burrows, M. da, G.M. Miguel, A.P. Varela, R.S. Becker, The aqueous solubility and thermal behaviour of some β-carbolines, Thermochim. Acta. 279 (1996) 77–82, https://doi.org/10.1016/S0040-6031(96)90063-5.
[75] G.T. Ruiz, G. Ferraudi, E. Wolcan, M.R. Féliz, On the elusive, non-emissive yet reactive, upper excited states of $[(4,4'\text{-bpy})Re^{I}(CO)_3(dppz)]PF_6$ (dppz=dipyridil [3,2-*a*:2′3′-*c*]phenazine), Inorganica Chim. Acta. 363 (2010) 1615–1618, https://doi.org/10.1016/j.ica.2010.01.033.
[76] M. Feliz, G. Ferraudi, Charge-Transfer Processes in (4-Nitrobenzoate)*Re*$(CO)_3(azine)_2$ Complexes. Competitive Reductions of 4-Nitrobenzoate and Azine in Thermally and Photochemically Induced Redox Processes, Inorg. Chem. 37 (1998) 2806–2810, https://doi.org/10.1021/ic971241j.
[77] J.C. Luong, L. Nadjo, M.S. Wrighton, Ground and excited state electron transfer processes involving *fac*-tricarbonylchloro(1,10-phenanthroline)rhenium(I). Electrogenerated chemiluminescence and electron transfer quenching of the lowest excited state, J. Am. Chem. Soc. 100 (1978) 5790–5795, https://doi.org/10.1021/ja00486a033.
[78] L. Sacksteder, M. Lee, J.N. Demas, B.A. DeGraff, Long-lived, highly luminescent rhenium(I) complexes as molecular probes: intra- and intermolecular excited-state interactions, J. Am. Chem. Soc. 115 (1993) 8230–8238, https://doi.org/10.1021/ja00071a036.
[79] F. Ragone, P.D. Gara, F.S. García Einschlag, A.G. Lappin, G.J. Ferraudi, E. Wolcan, G.T. Ruiz, Photophysics, photochemistry and thermally-induced redox reactions of a (Pterin)rhenium(I) complex, J. Photochem. Photobiol. A Chem. 358 (2018) 147–156, https://doi.org/10.1016/j.jphotochem.2018.02.015.
[80] E. Wolcan, Photosensitized generation of singlet oxygen from rhenium(I) complexes: a review, Inorganica Chim. Acta. 509 (2020), 119650, https://doi.org/10.1016/j.ica.2020.119650.